Atmos. Chem. Phys. Discuss., 12, 2483–2516, 2012
www.atmos-chem-phys-discuss.net/12/2483/2012/
doi:10.5194/acpd-12-2483-2012

Atmospheric Chemistry and Physics Discussions

Laboratory measurements and model sensitivity studies of dust deposition ice nucleation

G. Kulkarni, J. Fan, J. M. Comstock, X. Liu, and M. Ovchinnikov

Atmospheric Sciences and Global Change Division, Pacific Northwest National Laboratory, Richland, WA, 99352, USA

Received: 7 September 2011 – Accepted: 8 January 2012 – Published: 25 January 2012

Correspondence to: G. Kulkarni (gourihar.kulkarni@pnnl.gov)

Published by Copernicus Publications on behalf of the European Geosciences Union.

Abstract

We investigated the ice nucleating properties of mineral dust particles to understand the sensitivity of modeled cloud properties to different representations of contact angle in the Classical Nucleation Theory (CNT): onset single angle and probability density function (PDF) distribution approaches. These contact angle representations are based on two sets of laboratory deposition ice nucleation measurements: Arizona Test Dust (ATD) particles of 100, 300, and 500 nm sizes were tested at three different temperatures (−25, −30 and −35 °C), and 400 nm ATD and Kaolinite dust species were tested at two different temperatures (−30 and −35 °C). These measurements were used to derive the onset relative humidity with respect to ice (RH_{ice}) required to activate 1 % of dust particles as ice nuclei, from which the onset single contact angles were then calculated based on the CNT. For the PDF representation, parameters of the log-normal contact angle distribution (mean and standard deviation) were determined by fitting the CNT-predicted activated fraction to the measurements at different RH_{ice}. Results show that onset single contact angles are not much different between experiments, while the PDF parameters are sensitive to those environmental conditions (i.e., temperature and dust size). The cloud resolving model simulations show that cloud properties (i.e. ice number concentration, ice water content, and cloud initiation times) are sensitive to onset single contact angles and PDF distribution parameters, particularly to the mean value. The comparison of our experimental results with other studies shows that under similar measurement conditions the onset single contact angles are consistent within ±2.0°, while our derived PDF parameters have discrepancies.

1 Introduction

Ice containing clouds constitute one of the largest sources of uncertainty in predicting the Earth's climate according to the Intergovernmental Panel on Climate Change (IPCC) 2007 report (Forster et al., 2007). The uncertainty arises in part because of

ACPD
12, 2483–2516, 2012

the lack of understanding of the complex processes governing the formation of these clouds. Ice microphysics has important impacts on precipitation and Earth's radiative balance by altering cloud microphysical and radiative properties. Ice formation at temperatures below about −37 °C occurs via both homogeneous and heterogeneous ice nucleation mechanisms, while at warmer temperatures ice nucleation takes place only heterogeneously. Our understanding of homogeneous nucleation has improved dramatically over the last decades (e.g., Heymsfield and Miloshevich, 1995; Tabazadeh et al., 1997; Koop et al., 2000). Although advancements in heterogeneous ice nucleation observations and parameterizations have been reported (e.g., Kanji et al., 2011; Wang and Knopf, 2011; DeMott et al., 2010 and references therein), heterogeneous ice formation is still puzzling. There are at least two reasons why heterogeneous ice nucleation is much more complex than homogeneous freezing. First, it requires special atmospheric aerosols, called ice-forming nuclei (IN) (Pruppacher and Klett, 1997), which lower the free energy barrier for nucleation. Aerosol surface characteristics, such as morphology, solubility, active sites and epitaxial properties, have been postulated to play important roles in determining the ice nucleation efficiency of aerosol particles, but formulating a relationship among these characteristics has been difficult. Second, there are multiple heterogeneous ice nucleation mechanisms observed or hypothesized (Vali, 1985), such as deposition nucleation (ice formation directly from the vapor phase), condensation and immersion freezing (freezing initiated by the IN located within the supercooled water or solution droplet), and contact freezing (freezing occurring at the moment IN comes in contact with a supercooled water droplet or solution droplet). The relative importance of each mechanism in producing ice particles at given meteorological conditions is not well understood.

Although heterogeneous ice formation is complex, several parameterizations with or without a link to physiochemical properties (chemistry and surface characteristics) of an individual IN have been developed. These existing parameterizations can be broadly classified into two categories: empirical parameterizations that use laboratory or field measurements (e.g., Meyers et al., 1992; Diehl and Wurzler, 2004; Phillips et al., 2008;

ACPD
12, 2483–2516, 2012

DeMott et al., 2010), and those that are based on the classical nucleation theory (CNT) (e.g., Khvorostyanov and Curry, 2000, 2004; Liu and Penner, 2005). Empirical parameterizations are appealing because they are easy to implement and computationally efficient for coarse resolution regional/global models, but these schemes often have limited temperature and/or supersaturation ranges where they can be applied. In the CNT approach the nucleability of IN can be quantified in terms of aerosol properties such as contact angle. Contact angle of an ice embryo on an IN represents a relationship between the surface energies defined at the water vapor – liquid water, water vapor – ice and liquid water – ice interfaces. Several past studies have calculated the single value of contact angle under various ice nucleation conditions (e.g., Eastwood et al., 2008; Welti et al., 2009; Kanji and Abbatt, 2010; Kulkarni and Dobbie, 2010). This approach has the advantage that contact angle derived from various IN can be compared by formulating a deposition ice nucleation parameterization as a function of relative humidity (e.g., Wang and Knopf, 2011). Recently, it was even applied to the global climate model and used for long-term climate simulations (Hoose et al., 2010). It should be noted that other parameters in the CNT, e.g., the magnitudes of elastic strain, aerosol surface irregularities, active sites and pre-exponential constants will likely need to be constrained as they might be sensitive to the experimental conditions. These parameters are ignored in this study to simplify the computational task. We also recognize that previous studies (e.g., Connolly et al., 2009; Niedermeier et al., 2011) have formulated new parameterizations based on the ice-active surface site density approach, which is also not considered here.

The original framework of CNT can be generalized to incorporate the variability in surface properties of IN by assuming a probability density function (PDF) distribution of contact angles over the entire dust sample instead of single contact angle values (e.g., Marcolli et al., 2007). This modified approach using a log-normal PDF was employed by Lüönd et al. (2010) to show that laboratory immersion ice nucleation data can be used to constrain some of the CNT parameters, and the new approach can be used for representing ice nucleation in the climate models. However, such modifications to

ACPD
12, 2483–2516, 2012

incorporate the deposition ice nucleating properties into the CNT are missing. The ice nucleating properties are defined here as the fraction of dust particles nucleating ice as a function of relative humidity with respect to ice (RH_{ice}) at a given temperature (T) and particle size. Two empirical fits for the RH_{ice} dependence of deposition ice nucleation have been reported in the literature. Möhler et al. (2006) suggested the exponential fit framework, similar to Meyers et al. (1992), whereas Welti et al. (2009) suggested a sigmoidal fit curve. Both approaches were constrained using the laboratory measurement data. Welti et al. (2009) showed that the Möhler et al. (2006) approach does not fit their data well, possibly because of different measurement conditions and experimental techniques. These fit curve formulations can be further improved by finding a universal fit function that can be adapted to deposition ice nucleation measurements of various IN sizes as a function of T and RH_{ice}. Here we show that a modified CNT approach can be used to find such fit functions using the deposition ice nucleation measurements. The approach is based on the modified CNT approach of Lüönd et al. (2010), but the PDF distribution of contact angles is constrained by the laboratory data on deposition ice nucleation rather than immersion freezing.

In this study, we experimentally investigate the ice nucleating properties of mineral dust particles and examine the impact of the nucleation properties within the original and modified CNT framework on cloud properties simulated with a cloud resolving model (CRM). Two types of mineral dust particles are investigated for their nucleation properties: Arizona Test Dust (ATD) and Kaolinite. Deposition ice nucleation measurements of mineral dust particles were carried out using the ice chamber at Pacific Northwest National Laboratory (PNNL) Atmospheric Measurement Laboratory (AML). These measurements together with the data from past studies (Welti et al., 2009) are used to calculate the contact angles and PDF distributed contact angles. The sensitivity to these ice nucleating characteristics and broader implications of these CNT modifications are examined in the context of CRM simulated cloud properties: the ice number concentration (N_i), ice water content (IWC) and cloud evolution.

In the rest of the paper, Sect. 2 describes the experimental method to obtain the ice

ACPD
12, 2483–2516, 2012

nucleating properties of dust particles, presents the methodology for determining the PDF parameters from the contact angle distribution, and provides a description of the model and simulation cases. Section 3 includes the results of contact angle and PDF calculations using ice chamber measurements and a sensitivity analysis of the change in cloud properties to changes in the onset single contact angle and PDF parameters. The PDF parameters are also compared with the parameters derived from the literature data under similar measurement conditions (T, RH_{ice}, dust type and size). Finally, the summary and future research directions are presented in Sect. 4.

2 Methodology

2.1 Ice nucleation experiments

The experimental data on ice nucleation were obtained using the recently developed PNNL AML ice chamber. The basic design and functional details of the ice chamber are described in Stetzer et al. (2008) and Friedman et al. (2011). The chamber consists of two horizontal parallel plates that are independently T controlled and an evaporation section attached at the bottom of the chamber to remove water droplets (Stetzer et al., 2008). The principle of continuous flow water vapor diffusion chamber ensures aerosol particles that are placed between the layers of two sheath flows are exposed to constant T and RH_{ice} over the length of the chamber. The chamber wall temperatures are controlled using two external cooling baths (Lauda Brinkmann Inc.) and the T data are logged using the National Instrument CompactRIO programmable automation controller (cRIO-9114 combined with cRIO-9022). The chamber walls are coated with an ice layer (~ 0.5 mm thick) and a linear T gradient across the plates is created to produce a RH_{ice} profile between the plates. At the beginning of the experiment the temperature gradient is zero, which creates ice saturation conditions inside the chamber ($RH_{ice} = 100\,\%$), and then the refrigeration system cools one plate and warms the other to increase the RH_{ice}. The sheath and sample flow used are 10

ACPD
12, 2483–2516, 2012

and 1 Lpm, respectively, which limits the aerosol residence time to ∼ 12 s within the ice chamber. The aerosol particles on which ice forms under existing ice chamber measurement conditions (T and RH_{ice}) grow to a size greater than the original aerosol size and particles greater than 1 micrometers exiting the chamber are counted with an optical particle counter (OPC; CLiMET, model CI-3100) and classified as ice crystals. A schematic of the experimental setup is shown in Fig. 1.

The ATD (Powder Technology, Inc), a common surrogate for natural dust, is used in the first set of experiments. The second set of experiments with a Kaolinite (Sigma-Aldrich) dust sample is carried out to compare the results with the literature. The dust particles are dry-dispersed (TSI, 3433) and size-selected by a DMA (TSI, 3080). Different sizes of particles at 100 nm, 300 nm and 500 nm diameters, respectively are selected and forwarded to the ice chamber and Condensation Particle Counter (CPC; TSI, 3010). It was observed that selected size particle sample flow consists of multiple charged particles. For 100 nm size particles DMA produced 152 nm and 197 nm size particles and their contribution was 36 % and 16 %, respectively. For 300 nm and 500 nm size particles the contribution of multiple charged particles was less than 10 %. An active fraction (F_{ice}) is calculated as the ratio of number of ice crystals measured by the OPC to the total number of particles entering the chamber as measured by the CPC. F_{ice} calculations are corrected for the particle losses and RH_{ice} corrections, averaged over ±0.5 % relative humidity with respect to water (RH_w) and plotted as a function of RH_{ice} (shown in Fig. 2).

2.2 Modified classical nucleation theory

CNT provides a framework to parameterize deposition ice nucleation measurements. We adopt the PDF approach for contact angle from Lüönd et al. (2010) and calculate the PDF parameters using with deposition ice nucleation data from our laboratory. According to CNT, the nucleated fraction, F_{ice}, is given by

$$F_{ice} = 1 - \int_0^{\pi} p(\theta) \cdot \exp(-4\pi r^2 \cdot J(S_{v,i}, \theta) \cdot t) \cdot d\theta \quad (1)$$

ACPD
12, 2483–2516, 2012

where $p(\theta)$ is a lognormal PDF (Crowe, 2006) of contact angle, θ, given by

$$p(\theta) = \frac{1}{\theta\sigma\sqrt{2\pi}} \exp\left(-\frac{(\ln(\theta) - \ln(\mu))^2}{2\sigma^2}\right) \quad (2)$$

and the deposition nucleation rate, J, is given by Pruppacher and Klett (1997) and Fletcher (1962) as

$$J(S_{v,i}, \theta) = A_0 \cdot \exp\left(-\frac{16\pi M_w^2 \sigma_{i/v}^3}{3(RT\rho_i \ln S_{v,i})^2} \cdot \frac{f_{het}}{kT}\right) \quad (3)$$

where in Eqs. (1)–(3): r is the aerosol radius in meters, t is the aerosol residence inside the ice chamber in seconds, σ and μ are the logarithmic standard deviation and geometric mean of the PDF contact angle distribution, respectively, M_w is the molar mass of water ($= 0.018016\,\mathrm{kg\,mol^{-1}}$), $\sigma_{i/v}$ is the interfacial surface tension between the ice-vapor interface ($=0.106\,\mathrm{J\,m^{-2}}$), R is the universal gas constant ($= 8.314\,\mathrm{J\,K^{-1}\,mol^{-1}}$), $S_{v,i}$ is the supersaturation with respect to ice ($= \mathrm{RH_{ice}}\,(\%)/100 - 1$), k is the Boltzmann constant ($= 1.380622 \times 10^{-23}$, $\mathrm{J\,K^{-1}}$), f_{het} is the compatibility parameter given as $f_{het} = (2+m)(1-m)^2/4$, and m is defined as $\cos(\theta)$. Further the pre-exponential factor, A_0, ($= 10^{29}\,\mathrm{m^{-2}\,s^{-1}}$) is given by Pruppacher and Klett (1997),

$$A_0 = \frac{kT}{h} n \cdot \exp\left(\frac{-\Delta g}{kT}\right) \quad (4)$$

where n is the number density of water molecules at the ice nucleus/water interface, Δg is the activation energy for self-diffusion (or energy per bond in water), and h is the Planck constant.

The PDF approach assigns a single contact angle for each IN, and the probability of occurrence of these contact angles is given by a PDF distribution. The PDF distribution parameters, σ and μ (Eq. 1), are iterated to fit the experimental F_{ice} measurements

ACPD
12, 2483–2516, 2012

by minimizing the root mean square errors (RMSE) between the CNT calculated and measured F_{ice} values. An example of a PDF fit to the experimental data points and the associated PDF distribution are shown in Fig. 2. The square symbols show the experimental data obtained under the measurement conditions of −35 °C and 400 nm size ATD particles. A continuous fit curve (solid blue) is derived, and the nature of the fit curve (step) can be attributed to the non-linear nature of the Eqs. (1)–(3) in the calculations. The integral from (1) was discretized into 100 bins, further we did not find any sensitivity of bin width size towards the stepwise curve shape observed. The inset shows the PDF distribution and associated parameters. For the given conditions μ is 40.0° and σ is 0.3. The IN measurements are performed at various T using different dust sizes and the correspondingly calculated onset and PDF parameters are listed in Tables 1 and 3. Furthermore, (1) can be modified to calculate the onset single contact angles, which are based on the onset RH_{ice} (i.e., the value of RH_{ice} measured at 1 % F_{ice}) as per Lüönd et al. (2010). For these calculations the onset RH_{ice} values are directly read from the PDF modeled fitted curve. For example, the onset RH_{ice} for the data shown in Fig. 2 is ∼ 121 %. Both the original (single contact angle) and modified (PDF) versions of the CNT are tested as separate modules and also implemented into the CRM.

2.3 Description of model and the simulated case

The System for Atmospheric Modeling (SAM), coupled with a spectral-bin microphysical scheme (SBM) (Fan et al., 2009) was employed to simulate a mid-latitude stratiform and cirrus cloud case. SAM is a CRM with the dynamical framework of a large-eddy simulation (LES) model. The detailed SAM model description is given by Khairoutdinov and Randall (2003). The details about the SBM can be found in Khain et al. (2004) and Fan et al. (2009). Briefly, the SBM solves an equation system for eight number size distributions for water drops, ice crystals (columnar, plate-like, and dendrites), snowflakes, graupel, hail/frozen drops, and CCN. Each size distribution is represented by 33 mass doubling bins, i.e., the mass of a particle m_k in the k bin is determined

ACPD
12, 2483–2516, 2012

as $m_k = 2m_{k-1}$. All relevant microphysical processes/interactions including droplet nucleation, primary and secondary ice generation, condensation/evaporation of drops, deposition/sublimation of ice particles, freezing/melting, and mutual collisions between the various hydrometeors are calculated explicitly. The dependence of the collision efficiencies on height and the effects of turbulence on the rate of collisions are taken into account. An updated remapping scheme has been used that conserves three moments of the hydrometeor size distributions (concentration, mass, and radar reflectivity) to reduce spectral broadening and be more consistent with observations (Khain et al., 2008). The original and modified CNT parameterizations for deposition ice nucleation (as described in Sect. 2.2) are implemented into SAM-SBM for use in the sensitivity studies, with turning off all the other ice nucleation schemes in the SBM.

Two sets of model simulations are carried out to examine the sensitivity of modeled cloud properties to different representations of contact angles in the CNT. First, we test the original and modified CNT modules using fixed temperatures and RH_{ice}. The dust (IN) concentration (N_0), T, RH_{ice}, the integration time step and the contact angle information are the inputs to the modules. The initial dust size distribution employed in the model calculation is taken from Cziczo et al. (2006), with a N_0 of $10.7\,l^{-1}$. The N_0 was calculated by integrating the observed dust size distribution (Fig. 3). The tests are run with an N_0 of $10.7\,l^{-1}$ and a time step of 2 s for different contact angles and PDF parameters.

In the second set of model simulations, we conducted sensitivity studies using a CRM. The onset single contact angle is increased from 5 to 30° with an interval of 5°. CRM was also employed to perform a series of sensitivity tests by varying the PDF parameters. Finally, a sensitivity test to the initial N_0 is performed (Table 2) to compare the change in cloud properties caused by the initial N_0 with the fixed PDF parameters.

The cirrus cloud case observed from the US Department of Energy's Atmospheric Radiation Measurement (ARM) program at the South Great Plain (SGP) site in 9 March 2000 (Comstock et al., 2007) is chosen to test deposition freezing since the cloud

ACPD
12, 2483–2516, 2012

temperatures are colder than −22 °C. Simulations are run on a two-dimensional computational domain comprised of 72 horizontal grid points and 60 vertical layers with a horizontal resolution of 200 m and stretched vertical resolutions. Periodic lateral boundary conditions are used. The dynamic time step is 2 s. All simulations are run for 12 h, starting from 1500 on 9 March (UTC). The sounding and large-scale forcing data employed to drive the model are from the ARM Archive.

3 Results and discussion

3.1 Onset ice nucleation and PDF parameter calculations

The ice nucleating properties of different size ATD particles were investigated at various temperatures (Fig. 4). The results suggest that F_{ice} increases with RH_w showing dependency on T. For all the ATD sizes investigated, the general observation is that F_{ice} magnitudes at colder temperature (−30 and −35 °C) are larger than at −25 °C. Further, the ice nucleating properties of ATD and kaolinite dust particles of 400 nm size at −30 and −35 °C were also investigated (Fig. 5). The results show that F_{ice} increases with an increase in RH_w, similar to ice nucleating properties observed in Fig. 4.

We used F_{ice} data of ATD particles to illustrate the PDF fitted curve and corresponding PDF distribution. Figure 2 shows the change in F_{ice} as a function of RH_{ice} at −35 °C for ATD particles of 400 nm. The inset shows the PDF distribution and parameter magnitudes. The PDF parameters were also calculated for the other measurements, as shown in Tables 1 and 3. The tabulated results show that any statistical trend within PDF parameters cannot be drawn.

The scattering of the PDF parameters can be attributed to the distribution of active sites. The active sites are favored sites for ice nucleation (Pruppacher and Klett, 1997) and include characteristics such as surface irregularities, defects (e.g., Pruppacher and Klett, 1997; Welti et al., 2009) and chemical inhomogeneities (e.g., Chernoff and Bertram, 2010) that can promote to form the ice. These characteristics and

ACPD
12, 2483–2516, 2012

their activation efficiency as function of experimental parameters (T, RH_{ice} and r) differ from particle to particle, which results in the scattering of F_{ice} magnitudes (Figs. 2, 4 and 5) and therefore the scattering of PDF parameters. Recent studies (e.g., Cziczo et al., 2009; Eastwood et al., 2009; Chernoff and Bertram, 2010; Sullivan et al., 2010) of coating the particle with different chemical mixtures can minimize the role of aerosol substrate and subsequently the heterogeneity in the active sites. When the sites have different effectiveness of nucleating the ice, their randomness can be minimized by repeating the experiments at similar conditions. The PDF technique then can be applied to such measurements to investigate any statistical trend among PDF parameters.

The onset single contact angle can be assumed as a proxy of the IN forming ability and the results (Tables 1 and 3) indicate that the IN ability does not vary over the range of temperatures and three dust sizes studied here. It might be that the efficiency of active sites to nucleate dust particles at the onset conditions are similar, which is why we don't see any either T or size dependency on the onset conditions. The lack of T and size dependency could also be due to the experimental RH_{ice} uncertainty. For example, larger size particles could nucleate at lower onset RH_{ice} than smaller size dust particles due to the differences in surface area. However, if the difference between these two humidity values is less than the experimental RH_{ice} uncertainty ($\sim \pm 3\,\%$ in present study), then we would not be able to distinguish the size effect at onset conditions.

3.2 Sensitivity to contact angles derived from onset RH_{ice} and PDF approaches

The modeled ice number concentration (N_{ice}^{model}) results from the module tests of CNT responding to the onset single contact angles and PDF approaches are compared in Fig. 6. The tests are run for dust sizes of 100, 300 and 500 nm at temperatures of −25, −30, and −35 °C respectively initialized with N_0 ($= 10.7\,l^{-1}$) and at various RH_{ice} values 110 % to 150 % in the increment of 10 %. The results are extended into the water saturation regime just for illustration, showing N_{ice}^{model} from deposition ice nucleation mechanism only. In the water saturation regime we observed that both approaches

ACPD
12, 2483–2516, 2012

predict maximum N_{ice}^{model}, but only onset approach predicted N_{ice}^{model} equal to N_0. For all the simulations, at low humidity magnitudes the onset approach predicted zero N_{ice}^{model} and showed step function (jump in the N_{ice}^{model} from zero to maximum) with increase in the RH_{ice} except for Fig. 6a conditions. Whereas the PDF approach predicted non-zero N_{ice}^{model} and their magnitudes were lower than onset approach at all humidity values.

The sensitivity of N_{ice}^{model} as a function of RH_{ice} can be attributed to the representation method (single contact angle verses PDF) of ice nucleating properties. Onset single contact angles are calculated at one RH_{ice} magnitude, whereas the PDF approach uses many experimental data points to calculate the PDF parameters. For the same reason we think the onset approach predicted higher N_{ice}^{model}. In ice clouds, larger N_{ice}^{model} would result in smaller ice particle effective radius and an increase in cloud albedo. Consequently, the larger N_{ice}^{model} in models due to assumptions pertaining to IN could have a significant impact on cloud microphysical and radiative properties.

3.3 Cloud property sensitivity to the single contact angle and PDF parameters with CRM

Figure 7 shows the vertical profiles of N_i and IWC from the CRM simulations It is shown that both these cloud microphysical properties are sensitive to the change of contact angle, as contact angle increases, N_i and IWC decrease The maximum N_i and IWC occur at approximately 7.2 km altitude. At this height when contact angles increased from 5 to 30° both N_i and IWC decrease by 80 % and 30 %, respectively. The cloud thickness (Fig. 7b) is also sensitive to the contact angle: the contact angle increases the depth decreases.

Cloud initiation time is also sensitive to the contact angle as shown from the time-series of N_i (Fig. 8). The cloud structure (shape of the cloud and N_i) is similar over the entire simulation time as contact angles is increased from 5 to 10°. At some periods of evolution the N_i is equal to the N_0, meaning ice nucleation is very efficient for dust

ACPD
12, 2483–2516, 2012

with such low contact angles. When the contact angle is increased to 15°, the cloud initiation time is similar to the 5 and 10-degree simulations but the cloud structure is different. For clouds simulated at larger contact angles, i.e., at 20, 25 and 30°, the cloud initiation time is delayed by approximately 0.5, 3.8 and 6.0 h, respectively. In these three cases the N_i predicted is smaller than the N_0, suggesting lower nucleation rates for dust particles with larger contact angles. In general, cloud formation is delayed with the increase of contact angle.

Cloud sensitivity tests are also performed at various σ, μ and N_0 (Table 2). Three sets of tests are simulated: first we vary μ by fixing σ, then we vary σ by fixing μ, and in the third case we vary the N_0 with fixed σ and μ. Results indicate that cloud thickness is sensitive to μ and N_0 but not to σ (Fig. 9). The N_i and IWC averaged over the cloudy points are also more sensitive to μ than σ. As μ is decreased from 38.0 to 23.0°, N_i increases by more than 2–3 times and IWC by about 25 %, comparable to the increases resulted from about 9 times increase in N_0. Note that the cloud properties are only sensitive to the change of μ at some certain range: dramatic increases of cloud thickness, N_i and IWC are seen when μ is decreased from 28 to 23°. Both N_i and IWC are sensitive to the N_0 (Fig. 9c) and as expected an increase in the N_0 results in an increase of both N_i and IWC. Note that the simulated IWC (Fig. 9) is still much smaller than the retrieved values from the ground-based remote-sensing observations, especially above the height of 8.5 km. At these altitudes the temperatures are colder than −40 °C, and homogeneous freezing of aerosol could be the dominant mechanism as indicated by Sölch and Kärcher (2011). This ice formation mechanism is not considered in our tests. The main purpose here is to test the cloud sensitivity to different parameters for deposition freezing only, instead of producing a good simulation to match the observations, other three heterogeneous ice nucleation mechanisms are not simulated.

Based on the CNT, we know that the smaller contact angles correspond to the higher ice nucleation efficiency compared to the particles characterized by larger contact angles. For example, Chen et al. (2008) compared the contact angles for various particles

ACPD
12, 2483–2516, 2012

and in general mineral dust particles had smaller contact angles compared to uncoated soot particles. From the literature, we know that dust is a good IN (e.g. Möhler et al., 2006; Eastwood et al., 2008; Kanji and Abbatt, 2006; Welti et al., 2010) compared to uncoated soot (e.g., Dymarska et al., 2006; Koehler et al., 2009; Friedman et al., 2011) because it nucleates at relatively lower RH_{ice} at the same T. Cloud simulations show that it becomes more difficult to nucleate particles as the contact angle increases (Fig. 7a). Although our version of CNT does not directly include information of aerosol chemical composition and coating, the simulations with the larger contact angles can be associated with the particles that have suppressed ice nucleation ability, for example uncoated soot particles.

Similar argument can be surmised for describing the cloud initiation delay time with the increasing contact angles (Fig. 8). The particles that possess large contact angles are difficult to nucleate compared to those with smaller contact angles and can only nucleate after sufficient delay when particles would have more favorable ice nucleation conditions (i.e. colder T and higher RH_{ice}) in the atmosphere. A delay in cloud formation might also delay the onset of precipitation and a modification in cloud radiative forcing, which could produce a wide array of effects on weather and climate.

The decrease in μ results in a contact angle distribution that shifts towards smaller values, which leads to the larger N_i and IWC (Fig. 9a). The cloud depth also varies in these cases (Fig. 9), which would affect cloud radiative forcing and cloud lifetime. Based on the simulations presented here, we find that the σ is not as important as μ in terms of the effects on cloud properties. However, other extreme values of σ (e.g., σ equal to tenth of a percent) need to be investigated in the future to confirm our understanding. This information may help to simplify the relationship between the PDF parameters if we only need to include the variability of the μ parameter. In the last case (Fig. 9c) it is evident that as more particles are available to nucleate, under favorable ice nucleation conditions, would lead to the larger N_i and IWC. This simulation was carried out to understand the sensitivity of N_i and IWC to N_0 using fixed σ and μ. Although the sensitivities to the PDF parameters are conducted under the relatively low N_0 ($\sim 11\,l^{-1}$),

ACPD
12, 2483–2516, 2012

the results are not expected to change qualitatively at the higher N_0 since the fraction of activated IN is determined by the PDF parameters, not the N_0. Also, changing the breadth of dust distribution will certainly affect ice formation. But the results of the sensitivity to the PDF parameters are not expected to change qualitatively at different dust size distributions for the same reason.

3.4 PDF parameter comparison with the literature data

The PDF parameters can be used as a proxy for comparing the IN measurements. To illustrate the idea, ice nucleation measurements were carried out using ATD and Kaolinite dust particles at two different temperatures (Table 3) to compare the measurements with Welti et al. (2009). Keeping similar experimental conditions helped to compare the PDF parameters directly with each other. The comparison showed that there is a general agreement among the onset single contact angles, and these values are in agreement with the previous studies (Wang and Knopf, 2011 and references therein). But discrepancies exist within the PDF parameters, which could be attributed to the dust surface inhomogeneities, uncertainties within the measurements (e.g., RH_{ice}) and the ice chamber operational conditions (e.g., ice crystal detection threshold; bath cooling rates; see Sect. 2.1).

Recently, Kanji et al. (2011) reported the results from the Fourth International Ice Nucleation Workshop ICIS, 2007. The results indicate good agreement between the IN measurements carried out by the three different ice chamber instruments; however absolute differences in terms of calculated onset T and RH_{ice} were noted. The study highlighted the importance of ice crystal detection threshold, experimental flow technique and low T kinetic effects on the IN measurements. Similar arguments can be suggested in our study that might have contributed to the discrepancy in the PDF parameters, except that the ice chamber geometry was similar (Sect. 2.1). Other factors such as dust surface area and chemistry, and errors in the IN measurements could also have played a role. We think minimizing the contribution from these factors would help to compare the IN measurements in future.

ACPD
12, 2483–2516, 2012

4 Summary and future work

Deposition ice nucleation experiments are carried out to investigate the ice nucleating properties of 100, 300, 400 and 500 nm size dust particles at −25, −30 and −35 °C temperatures. The CNT framework was modified by implementing a PDF contact angle distribution approach and the PDF parameters are constrained using these measurements. The CNT is parameterized using single contact angle and PDF approaches and are implemented into a CRM to examine the sensitivity of cloud properties (N_i, IWC and cloud initiation time). The main conclusions from this study are as follows:

1. In the module tests of CNT, larger N_{ice}^{model} are observed with the onset single contact angle approach compared with the PDF representation, which could result in smaller ice crystals radius and might affect cloud microphysical and radiative properties.

2. An increase in the contact angle results in a decrease in N_i and IWC. Also the cloud initiation time is delayed by ∼ 6 h when the contact angles are increased from 5 to 30°. Cloud properties are found to be sensitive to contact angle with a single contact angle approach.

3. Both N_i and IWC increase with a decrease in the μ, while they are not sensitive to the σ. As μ decreases from 38 to 23°, N_i increases by more than 2–3 times and IWC increases by about 25 %. Modeled cloud properties are highly sensitive to the change of μ within a certain range: dramatic increases of cloud thickness, N_i and IWC are seen when μ is decreased from 28 to 23°. As expected, N_i and IWC increase with an increase of N_0. Overall, this implies that the cloud properties are sensitive to the PDF parameters.

4. Onset single contact angles are observed to be consistent with the literature data, but discrepancies within the PDF parameters exist. Definite reasons for the discrepancy cannot be understood at this time, but several factors like dust physiochemical properties and IN measurement procedure might be responsible.

ACPD
12, 2483–2516, 2012

Cloud properties are observed sensitive to the magnitude and representation method of contact angles, implying that accurate representation of contact angle is crucial to simulate cloud properties in the model. Therefore, experimental methods applied to obtain the contact angles need to be standardized in the future (Cantrell and Heymsfield, 2005).

There are number of previous studies (e.g., Möhler et al., 2006; Welti et al., 2009; Kulkarni and Dobbie, 2010; Jones et al., 2011) that have investigated the ice nucleating properties of various dust types. These available measurements can be used to calculate the PDF parameters and a matrix of such PDF parameters then can be examined for a relationship to simplify the parameterization task. The task can be further improved by employing quality controlled data sets, e.g. incorporating experimental measurement errors and larger particle size data that has limited multiple charge particle influence, from different ice nucleation research groups to calculate the PDF parameters that can be compared with one another to understand the ice nucleating properties of aerosol particles. In future new approaches such as ice-active surface site density approach (e.g., Connolly et al., 2009) should be explored to fit the laboratory data and incorporated in the modeling studies to understand the importance of such approach towards simulating the cloud properties.

Acknowledgements. We acknowledge the support from PNNL Aerosol-Climate Initiative (ACI). We thank Steven Ghan and Andrew Welti for the project support and providing laboratory data, respectively. The Pacific Northwest National Laboratory is operated for DOE by Battelle Memorial Institute under contract DE-AC06-76RLO 1830. We also thank three anonymous reviewers for providing the important comments, which have helped to improve the quality of the manuscript.

References

Chen, J.-P., Hazra, A., and Levin, Z.: Parameterizing ice nucleation rates using contact angle and activation energy derived from laboratory data, Atmos. Chem. Phys., 8, 7431–7449, doi:10.5194/acp-8-7431-2008, 2008.

ACPD
12, 2483–2516, 2012

Chernoff, D. I. and Bertram, A. K.: Effects of sulfate coatings on the ice nucleation properties of a biological ice nucleus and several types of minerals, J. Geophys. Res., 115, D20205, doi:10.1029/2010JD014254, 2010.

Comstock J. M., D'Entremont, R., De Slover, D., Mace, G. G., Matrosov, S. Y., McFarlane, S. A., Minnis, P., Mitchell, D., Sassen, K., Shupe, M. D., Turner, D. D., and Wang, Z.: An intercomparison of microphysical retrieval algorithms for upper-tropospheric ice clouds, B. Am. Meteorol. Soc., 88, 191–204, 2007.

Connolly, P. J., Möhler, O., Field, P. R., Saathoff, H., Burgess, R., Choularton, T., and Gallagher, M.: Studies of heterogeneous freezing by three different desert dust samples, Atmos. Chem. Phys., 9, 2805–2824, doi:10.5194/acp-9-2805-2009, 2009.

Crowe, C. T.: Multiphase Flow Handbook, CRC Press, USA, 2006.

Cziczo D. J., Thomson, D. S., Thompson, T. L., DeMott, P. J., and Murphy, D. J. M.: Particle analysis by laser mass spectrometry (PALMS) studies of ice nuclei and other low number density particles, Int. J. Mass Spectrom., 258, 21–29, 2006.

Cziczo D. J., Froyd, K. D., Gallavardin, S. J., Moehler, O., Benz, S., Saathoff, H., and Murphy, D. M.: Deactivation of ice nuclei due to atmospherically relevant surface coatings, Environ. Res. Lett., 4, 044013, doi:10.1088/1748-9326/4/4/044013, 2009.

DeMott, P. J., Prenni, A. J., Liu, X., Kreidenweis, S. M., Petters, M. D., Twohy, C. H., Richardson, M. S., Eidhammer, T., and Rogers, D. C.: Predicting global atmospheric ice nuclei distributions and their impacts on climate, P. Natl. Acad. Sci. USA, 107, 11217–11222, 2010.

Dymarska, M., Murray, B. J., Sun, L. M., Eastwood, M. L., Knopf, D. A., and Bertram, A. K.: Deposition ice nucleation on soot at temperatures relevant for the lower troposphere, J. Geophys. Res., 111, D04204, doi:10.1029/2005JD006627, 2006.

Eastwood, M. L., Cremel, S., Gehrke, C., Girard, E., and Bertram, A. K.: Ice nucleation on mineral dust particles: onset conditions, nucleation rates and contact angles, J. Geophys. Res., 113, D22203, doi:10.1029/2008JD010639, 2008.

Fan, J., Ovtchinnikov, M., Comstock, J., McFarlane, S. A., and Khain, A.: Ice formation in Arctic mixed-phase clouds: insights from a 3-D cloud-resolving model with size-resolved aerosol and cloud microphysics, J. Geophys. Res., 114, D04205, doi:10.1029/2008JD010639, 2009.

Fletcher, N. H.: Physics of Rainclouds, Cambridge University Press, Cambridge, 1962.

Forster, P. M., Ramaswamy, V., Solomon, S., Qin, D., Manning, M., Chen, Z., Marquis, M., Averyt, K., Tignor, M., Miller, H. L., (Ed): Changes in atmospheric constituents and in radiative forcing, in: Climate Change 2007: The Physical Science Basis. Contribution of

ACPD
12, 2483–2516, 2012

Working Group I to the Fourth Assessment Report of the Intergovernmental Panel on Climate Change, edited by: Solomon, S., Qin, D., Manning, M., Chen, Z., Marquis, M., Averyt, K., Tignor, M., and Miller, H. L., Cambridge University Press, 2007.

Friedman, B., Kulkarni, G., Beránek, J., Zelenyuk, A., Thornton, J., and ziczo, D.: Ice nucleation and droplet formation by bare and coated soot particles, J. Geophys. Res., 116, D17203, doi:10.1029/2011JD015999, 2011.

Heymsfield, A. J. and Miloshevich, L. M.: Relative humidity and temperature influences on cirrus formation and evolution: observations from wave clouds and FIRE II, J. Atmos. Sci., 52, 4302–4326, 1995.

Kanji, Z. A. and Abbatt, J. P. D.: Laboratory studies of ice formation via deposition mode nucleation onto mineral dust and n-hexane soot samples, J. Geophys. Res., 111, D16204, doi:10.1029/2005JD006766, 2006.

Kanji, Z. A. and Abbatt, J. P. D.: Ice nucleation onto arizona test dust at cirrus temperatures: effect of temperature and aerosol size on onset relative humidity, J. Phys. Chem. A, 114, 935–941, 2010.

Kanji, Z. A., DeMott, P. J., Möhler, O., and Abbatt, J. P. D.: Results from the University of Toronto continuous flow diffusion chamber at ICIS 2007: instrument intercomparison and ice onsets for different aerosol types, Atmos. Chem. Phys., 11, 31–41, doi:10.5194/acp-11-31-2011, 2011.

Khain, A., Pokrovsky, P. A., Pinsky, M., Seifert, A., and Phillips, V.: Simulation of effects of atmospheric aerosols on deep turbulent convective clouds using a spectral microphysics mixed-phase cumulus cloud model: I. Model description and possible applications, J. Atmos. Sci., 61, 2963–2982, 2004.

Khain, A., BenMoshe, N., and Pokrovsky, A.: Factors determining the impact of aerosols on surface precipitation from clouds: an attempt at classification, J. Atmos. Sci., 65, 1721–1748, 2008.

Khairoutdinov, M. F. and Randall, D. A.: Cloud resolving modeling of the ARM summer 1997 IOP: model formulation, results, uncertainties, and sensitivities, J. Atmos. Sci., 60, 607–625, 2003.

Khvorostyanov, V. I. and Curry, J. A.: A new theory of heterogeneous ice nucleation for application in cloud and climate models, Geophys. Res. Lett., 27, 4081–4084, 2000.

Khvorostyanov, V. I. and Curry, J. A.: The theory of ice nucleation by heterogeneous freezing of deliquescent mixed CCN. Part 1: Critical radius, energy and nucleation rate, J. Atmos. Sci.,

ACPD
12, 2483–2516, 2012

61, 2676–2691, 2004.
Koehler, K. A., DeMott, P. J., Kreidenweis, S. M., Popovicheva, O. B., Petters, M. D., Carrico, C. M., Kireeva, E. D., Khokhlova, T. D. and Shonija, N. K.: Cloud condensation nuclei and ice nucleation activity of hydrophobic and hydrophilic soot particles, Phys. Chem. Chem. Phys., 11, 7906–7920, 2009.
Koop, T., Luo, B., Tsias, A., and Peter, T.: Water activity as the determinant for homogeneous ice nucleation in aqueous solutions, Nature, 406, 611–614, 2000.
Kulkarni, G. and Dobbie, S.: Ice nucleation properties of mineral dust particles: determination of onset RH*i*, IN active fraction, nucleation time-lag, and the effect of active sites on contact angles, Atmos. Chem. Phys., 10, 95–105, doi:10.5194/acp-10-95-2010, 2010.
Liu, X. and Penner, J.: Ice nucleation parameterization for global models, Meteorol. Z., 14, 499–514, 2005.
Lüönd, F., Stetzer, O., Welti, A., and Lohmann, U.: Experimental study on the ice nucleation ability of size-selected kaolinite particles in the immersion mode, J. Geophys. Res., 115, D14201, doi:10.1029/2009JD012959, 2010.
Marcolli, C., Gedamke, S., Peter, T., and Zobrist, B.: Efficiency of immersion mode ice nucleation on surrogates of mineral dust, Atmos. Chem. Phys., 7, 5081–5091, doi:10.5194/acp-7-5081-2007, 2007.
Meyers M. P., DeMott P. J., and Cotton W. R.: New primary ice-nucleation parameterizations in an explicit cloud model, J. Appl. Meteorol., 31, 708–721, 1992.
Möhler, O., Field, P. R., Connolly, P., Benz, S., Saathoff, H., Schnaiter, M., Wagner, R., Cotton, R., Krämer, M., Mangold, A., and Heymsfield, A. J.: Efficiency of the deposition mode ice nucleation on mineral dust particles, Atmos. Chem. Phys., 6, 3007–3021, doi:10.5194/acp-6-3007-2006, 2006.
Niedermeier, D., Shaw, R. A., Hartmann, S., Wex, H., Clauss, T., Voigtländer, J., and Stratmann, F.: Heterogeneous ice nucleation: exploring the transition from stochastic to singular freezing behavior, Atmos. Chem. Phys., 11, 8767–8775, doi:10.5194/acp-11-8767-2011, 2011.
Phillips V. T. J., DeMott P. J., and Andronache, C.: An empirical parameterization of heterogeneous ice nucleation for multiple chemical species of aerosol, J. Atmos. Sci., 65, 2757–2783, 2008.
Pruppacher, H. R. and Klett, J. D.: Microphysics of Clouds and Precipitation, Springer Publications, New York, 1997.

ACPD
12, 2483–2516, 2012

Richardson, M. S., DeMott, P. J., Kreidenweis, S. M., Cziczo, D. J., Dunlea, E. J., Jimenez, Thomoson, D. S., Ashbaugh, L. L., Borys, R. D., Westphal, D. L., Casuccio, G. S., and Lersch, T. L.: J. Geophys. Res., 112, D02209, doi:10.1029/2006JD007500, 2007.

Sölch I. and Kärcher, B.: Process-oriented large-eddy simulations of a midlatitude cirrus cloud system based on observations, Q. J. Roy. Meteor. Soc. 137, 374–393, 2011.

Stetzer, O., Baschek, B., Luond, F., and Lohmann, U.: The Zurich Ice Nucleation Chamber (ZINC) – a new instrument to investigate atmospheric ice formation, Aerosol Sci. Technol. 42, 64–74, 2008.

Sullivan, R. C., Petters, M. D., DeMott, P. J., Kreidenweis, S. M., Wex, H., Niedermeier, D., Hartmann, S., Clauss, T., Stratmann, F., Reitz, P., Schneider, J., and Sierau, B.: Irreversible loss of ice nucleation active sites in mineral dust particles caused by sulphuric acid condensation, Atmos. Chem. Phys., 10, 11471–11487, doi:10.5194/acp-10-11471-2010, 2010.

Tabazadeh, A., Jensen, E. J., and Toon, O. B.: A model description for cirrus cloud nucleation from homogeneous freezing of sulfuric acid aerosols, J. Geophys. Res., 102, 23845–23850, 1997.

Vali, G.: Nucleation terminology, B. Am. Meteorol. Soc., 66, 1426–1427, 1985.

Wang, B. and Knopf, D. A.: Heterogeneous ice nucleation on particles composed of humic-like substances impacted by O_3, J. Geophys. Res., 116, D03205, doi:10.1029/2010JD014964, 2011.

Welti, A., Lüönd, F., Stetzer, O., and Lohmann, U.: Influence of particle size on the ice nucleating ability of mineral dusts, Atmos. Chem. Phys., 9, 6705–6715, doi:10.5194/acp-9-6705-2009, 2009.

ACPD
12, 2483–2516, 2012

Table 1. PDF parameters and onset ice nucleation conditions investigated at several temperatures and dust sizes. The range of onset θ variation was minimum compared to the μ parameter.

Dust size	100 nm			300 nm			500 nm		
T (°C)	−25	−30	−35	−25	−30	−35	−25	−30	−35
μ (deg)	56.0	38.0	38.0	27.0	57.0	36.0	45.0	64.0	32.0
σ	0.31	0.21	0.19	0.05	0.29	0.19	0.25	0.41	0.12
Onset RH_{ice} (%)	132	130	131	130	126	125	128	127	126
Onset θ (deg)	23.0	24.0	24.0	22.5	22.0	22.0	22.5	23.0	21.0

ACPD
12, 2483–2516, 2012

Table 2. Cloud sensitivity tests of μ (deg), σ and N_0 (l^{-1}) variables. Three cases were simulated. In the case 3 simulations the parameters μ and σ are 33.0 and 0.41 respectively were held constant.

Case 1		Case 2		Case 3	
Simulations	μ with $\sigma = 0.14$	Simulations	σ with $\mu = 23.0$	Simulations	N_0
MU1	38.0	SD1	0.14	IN0	$N = 10.7 l^{-1}$
MU2	33.0	SD2	0.22	IN1	$3 \times N_0$
MU3	28.0	SD3	0.30	IN2	$6 \times N_0$
MU4	23.0	SD4	0.38	IN3	$10 \times N_0$
MU5	18.0	–	–	–	–

ACPD
12, 2483–2516, 2012

Table 3. Comparison of derived PDF parameters calculated at two temperatures and dust types (of size 400 nm) with Welti et al. (2009). Possible sources of disagreement are outlined in the text. The data highlighted in bold are used to plot the PDF distribution shown in Fig. 2.

Group	Present study				Welti et al. (2009)			
Dust	**ATD**		Kaolinite		ATD		Kaolinite	
T (°C)	−30	**−35**	−3	−35	−3	−35	−3	−35
μ (deg)	33.0	**40.0**	62.0	56.0	40.0	22.0	58.0	28.0
σ	0.21	**0.30**	0.5	0.49	0.295	0.065	0.36	0.29
Onset RH_{ice} (%)	117	121	121	115	121	120	130	112
Onset θ (deg)	18.0	20.0	20.0	17.5	20.0	20.0	23.0	17.0

ACPD
12, 2483–2516, 2012

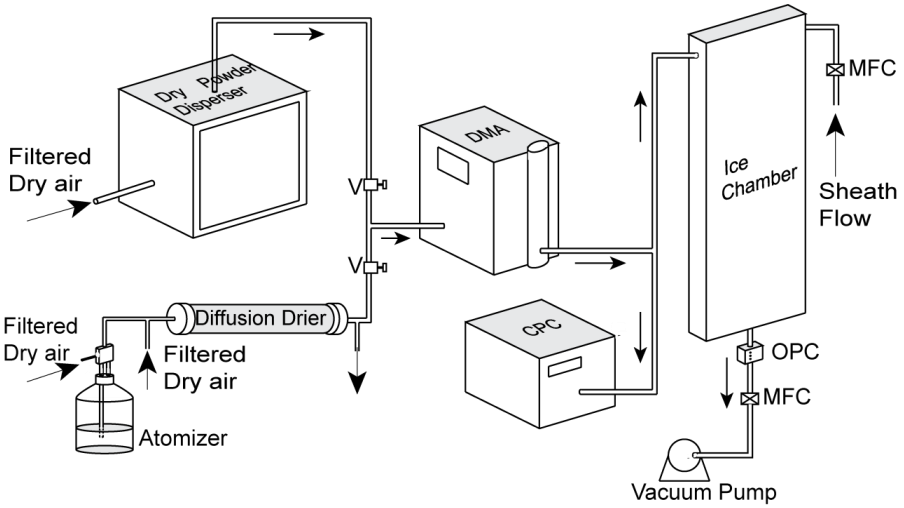

Fig. 1. Experimental setup used to determine the IN fraction of dust particles. The ATD particles are dry dispersed and size selected and investigated for their ice nucleation efficiency. The atomizer set up is used to validate the T and RH_{ice} conditions within the ice chamber (data not shown here). The polydisperse particles of ammonium sulfate are generated in the atomizer, and passed through the drier to remove any water droplets and water residing on the ammonium sulfate particles. The sample flow is forwarded to the DMA and consequently to ice chamber and CPC. The remainder of the flow went to the exhaust. The valve (V) was used to switch between these two types of experiments. The mass flow controller (MFC) was used to regulate the ice chamber flows.

ACPD
12, 2483–2516, 2012

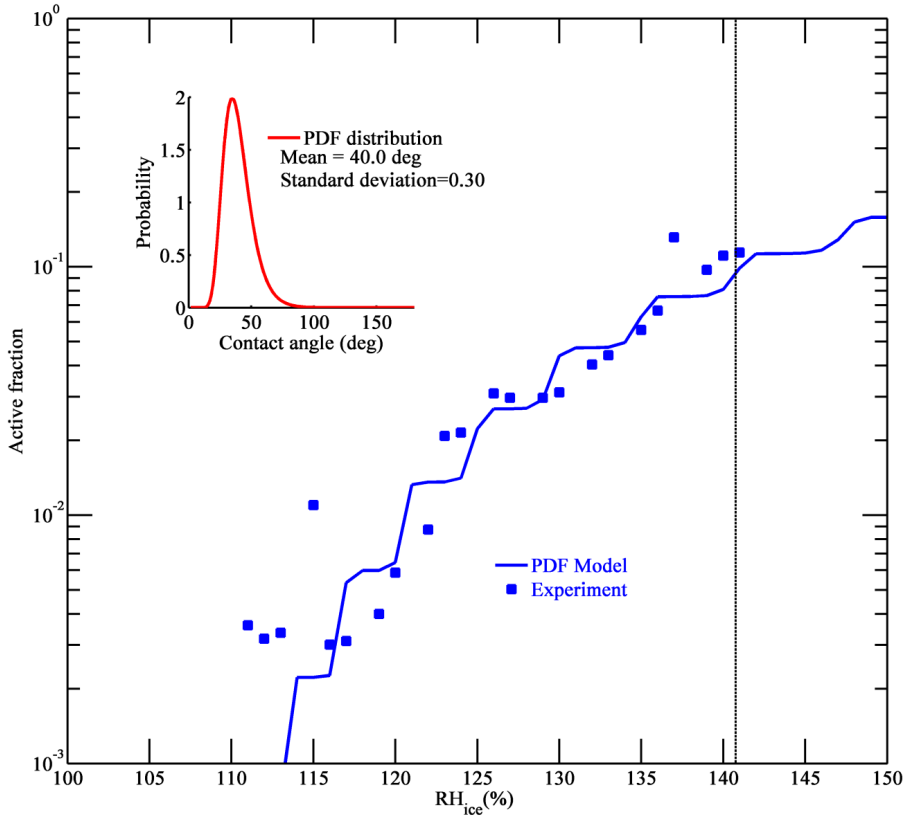

Fig. 2. Active fraction of ATD particles as a function RH_{ice}. The experiment was carried out at −35 °C and using size of 400 nm (Table 3). The solid curve shows the PDF model fit to the experimental data points. The inset shows the PDF distribution with corresponding parameters. Vertical dashed line indicates the water saturation. The error for RH_{ice} is approximately ±3 %.

ACPD
12, 2483–2516, 2012

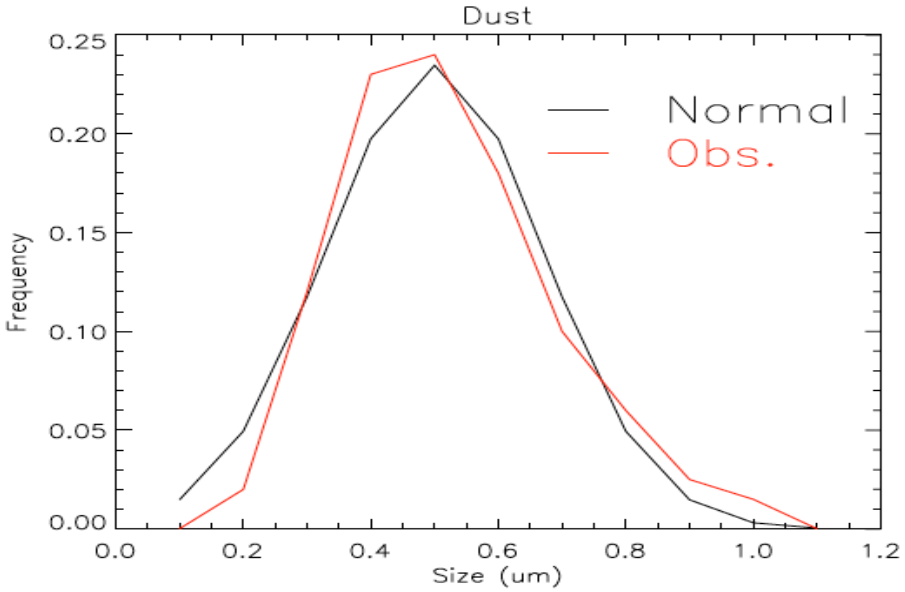

Fig. 3. The normalized size distribution observed in Cziczo et al., 2006 (red) and the fitted normal distribution used in the model simulations (black). The integrated dust number concentration N_0 is 10.7 l^{-1}.

ACPD
12, 2483–2516, 2012

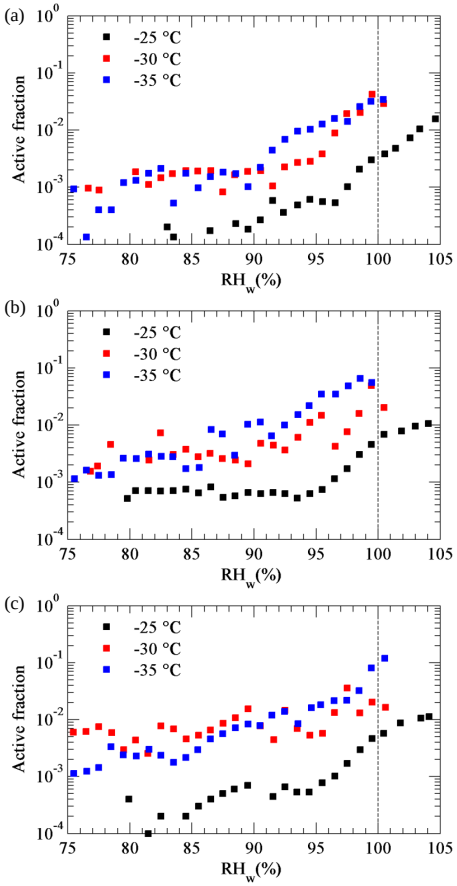

Fig. 4. Active fraction of ATD particles as a function of RH_w(%). Three different size particles were investigated at −25, −30 and −35 °C temperatures. Panel **(a)**, **(b)** and **(c)** corresponds to the 100 nm, 300 nm and 500 nm size particles, respectively. Vertical dashed line represents the water saturation.

ACPD
12, 2483–2516, 2012

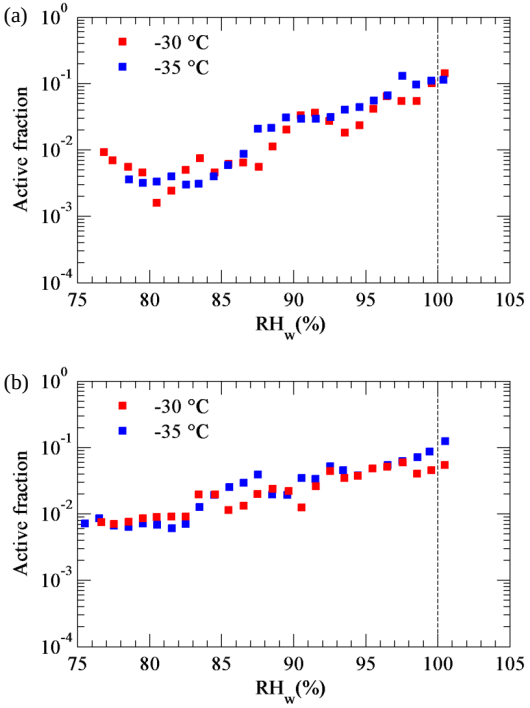

Fig. 5. Active fraction of 400 nm size **(a)** ATD and **(b)** kaolinite particles as a function of RH_w (%). The particles were investigated at −30 and −35 °C temperatures. Vertical dashed line represents the water saturation.

ACPD
12, 2483–2516, 2012

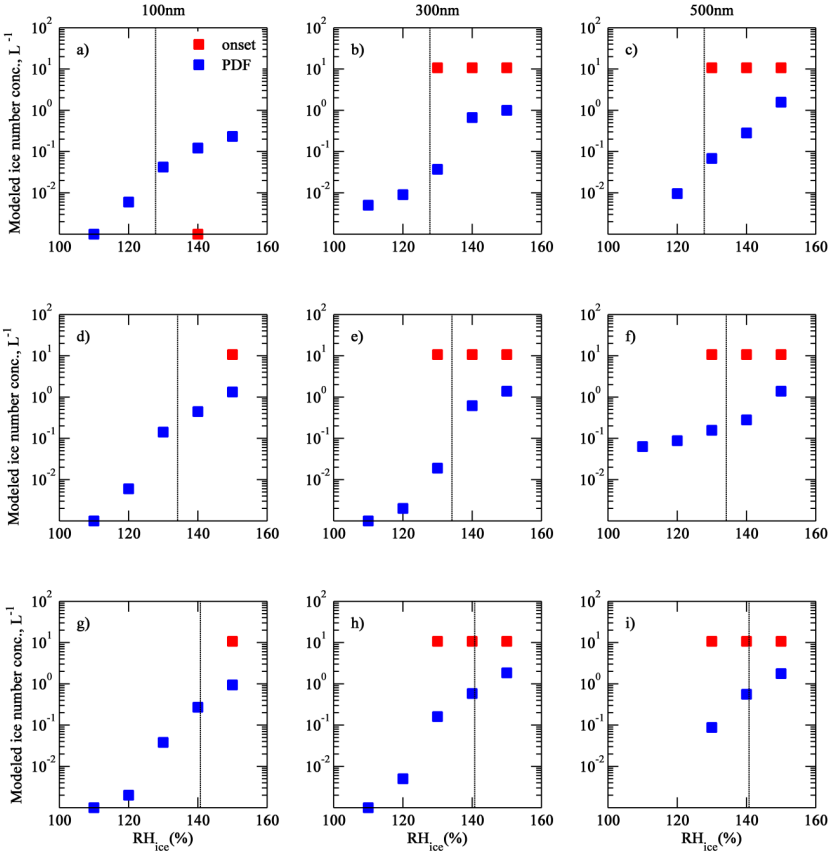

Fig. 6. Comparison of N_{ice}^{model} calculated by the onset RH_{ice} and PDF approaches under various IN measurement conditions (Table 1). Panels **(a)** to **(c)**, **(d)** to **(f)** and **(g)** to **(i)** correspond to −25, −30 and −35 °C, respectively. Vertical dashed line represents the water saturation line. PDF calculations are extended into water saturation regime only for the illustration.

ACPD
12, 2483–2516, 2012

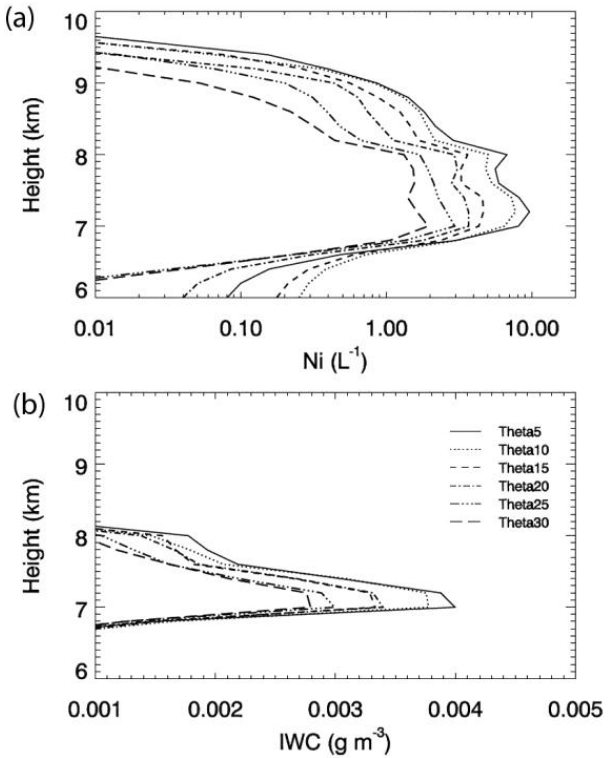

Fig. 7. Domain and time averaged **(a)** vertical profiles of N_i and **(b)** IWC simulated in the CRM. Increase in the contact angles (shown as ThetaX, where X is contact angle in degrees) results in the decrease of N_i and IWC.

ACPD
12, 2483–2516, 2012

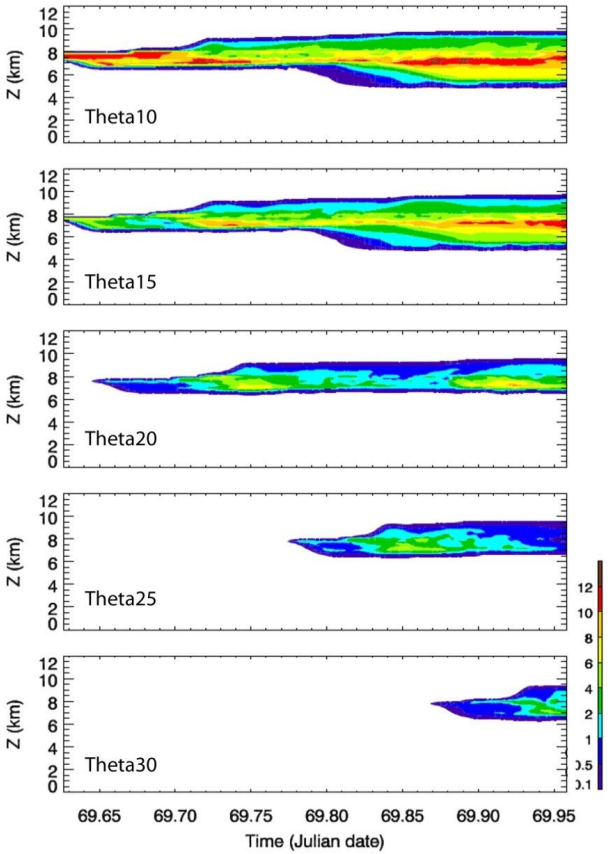

Fig. 8. Time series of vertical profile of cloud N_i (domain-average) simulated using CRM. The total cloud evolution time simulated was ~8 h. Each panel shows the cloud structure under different onset single contact angle (shown as ThetaX, where X is contact angle in degrees). The N_0 was 10.7 l^{-1} in each case. The cloud structure and initiation time are observed to be sensitive to the contact angles.

ACPD
12, 2483–2516, 2012

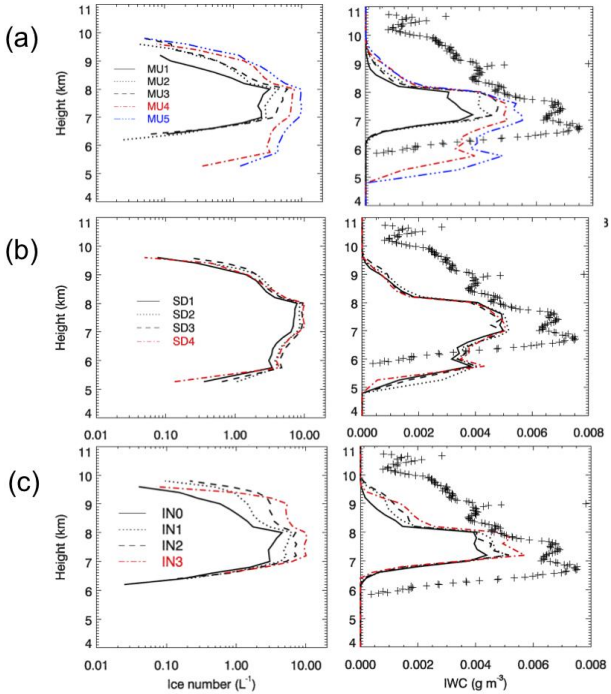

Fig. 9. N_i and IWC averaged over the cloudy-points from the sensitivity tests of **(a)** μ (MU), **(b)** σ (SD), and **(c)** N_0 simulated in the CRM. See Table 2 for details. The observed IWC (+) was retrieved from the ground-based lidar and radar observations (Comstock et al., 2007).

ACPD
12, 2483–2516, 2012